Electronic Supplementary Material (ESI) for Materials Chemistry Frontiers.

Supporting Information

Boosting the overall specific capacity of SiO electrodes for lithium-ion batteries using a multifunctional carbon cloth current collector

Hao Chen[a,b,*,†], Jiajie Wang[b,†], Ziheng Guan[b], Yingjie Tao[b], Lanze Li[b], Junjie Wei[b], Shijie Ma[b], Zhilin Yan[a], Jing Han[b], Fan Wang[b,*], Zhehong Shen[b], and Deren Yang[a]

[a] State Key Laboratory of Silicon and Advanced Semiconductor Materials and School of Materials Science and Engineering, Zhejiang University, Hangzhou 310027, People's Republic of China

[b] College of Chemistry and Materials Engineering, Zhejiang A&F University, Hangzhou 311300, People's Republic of China.

Corresponding authors. E-mail: haochen@zafu.edu.cn (H. Chen); wangf@zafu.edu.cn (F. Wang)

[†] These two authors contributed equally to this work.

1. Chemicals and reagents

Acetone (C_3H_6O, AR, 99%) was purchased from Shanghai Chemical Reagent Co., Ltd. (PR China). Anhydrous ethanol (C_2H_6O, AR) was purchased from Shanghai Aladdin Biochemical Technology Co., Ltd. (PR China). SiO (SiO, 99.9%, AM-SiO-001-3, D (50) = 1.09 μm) was purchased from Nangong City Bole Metal Materials Co., Ltd. (PR China). Hydrophilic carbon cloth (W0S1011, see Table S1), hydrophobic carbon cloth (W1S1011), and carbon paper (GDS180S) purchased from CeTech Co., Ltd. Acetylene black (F-900) purchased from Tianjin Yiborui Chemical Co., Ltd. (PR China). Sodium carboxymethyl cellulose (CMC, 99.8%), copper foil (Cu foil, 99.9%), lithium iron phosphate (LFP-1, power type, 99.8%), N-methyl pyrrolidone (NMP, battle grade, 99.9%), polyvinylidene fluoride (PVDF, HSV900), aluminum foil (Al foil, 99.9%) purchased from Taiyuan Lizhiyuan Technology Co., Ltd. (PR China). The electrolyte (1 M $LiPF_6$ dissolved in a 1: 1 volume mix of ethylene carbonate (EC)/diethylene carbonate (DEC) with 5% ethylene fluoro carbonate (FEC)) was purchased from Suzhou Industrial Park Sange Chemical Technology Co., Ltd. (PR China). All reagents and materials were used directly without any treatment.

Table S1. Properties of W0S1011 hydrophilic carbon cloth

Properties	Units	Method	Parameter
Elemental Composition	%	TSL, AMETEK	C: 96%, N: 3%, O: 1%
Air Permeability	sec	Gurley	＜10
Tensile Strength (MD)	N/cm	ASTM D-828	10
Tensile Strength (XD)	N/cm	ASTM D-828	5

2. Detailed evaluation process of Li^+ diffusion coefficient

For the galvanostatic intermittent titration technique (GITT) test, cells were charged and discharged at a current density of 100 mA g^{-1} for 10 min and left to stand for 30 min. The diffusion coefficient can be calculated based on $D_{Li^+}=(4/\pi\tau) \times (m_B V_M/(M_B S))^2 \times (\Delta E_s/\Delta E_\tau)^2$, where D_{Li^+} is the Li^+ diffusion coefficient (cm^{-2} s^{-1}), τ is the duration of current pulse (10 min), m_B (g) and M_B (g mol^{-1}) are the mass and molecular weight of the active materials in the electrode, respectively, V_M (cm^3 mol^{-1}) and S (cm^{-2}) are the molar volume and the total area of the electrode, respectively, and ΔE_τ and ΔE_s are the changes in the cell voltage during the 10 min current pulse from τ_0 to τ_{0+t} and the relaxation period of 30 min, respectively. The Li^+ diffusion coefficient was also investigated by the CV method according to $D_{Li^+}=I2\ PRT/(0.1992\times F^3S^2C2\ ov)$, $I_P=(D_{Li^+}\times 0.1992\times F^3S^2C2\ o/(RT))^{1/2}v^{1/2}$, and $k=(D_{Li^+}\times 0.1992\times F^3S^2C2\ o/(RT))^{1/2}$, where I_P is the current peak intensity (mA), R (J $K^{-1}mol^{-1}$) is the gas constant, T (K) is the temperature, F (C mol^{-1}) is the Faraday constant, S is the electrode surface area (1.13 cm^2), C_o is the molar concentration of lithium ions in the material (mol cm^{-3}), v is the scan rate (mV s^{-1}), and k is the slope of the fitting curve.[1-3]

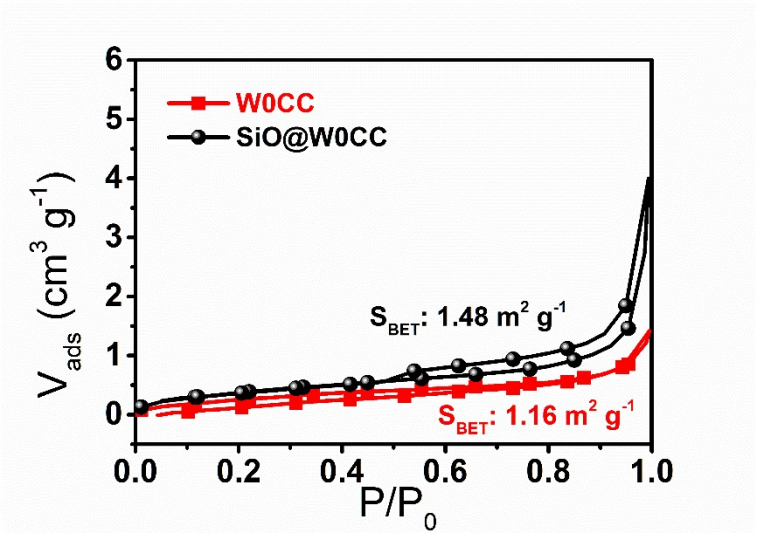

Figure S1. N_2 adsorption-desorption curves of W0CC and SiO@W0CC electrode with the SiO loading density of 0.9 mg cm^{-2}.

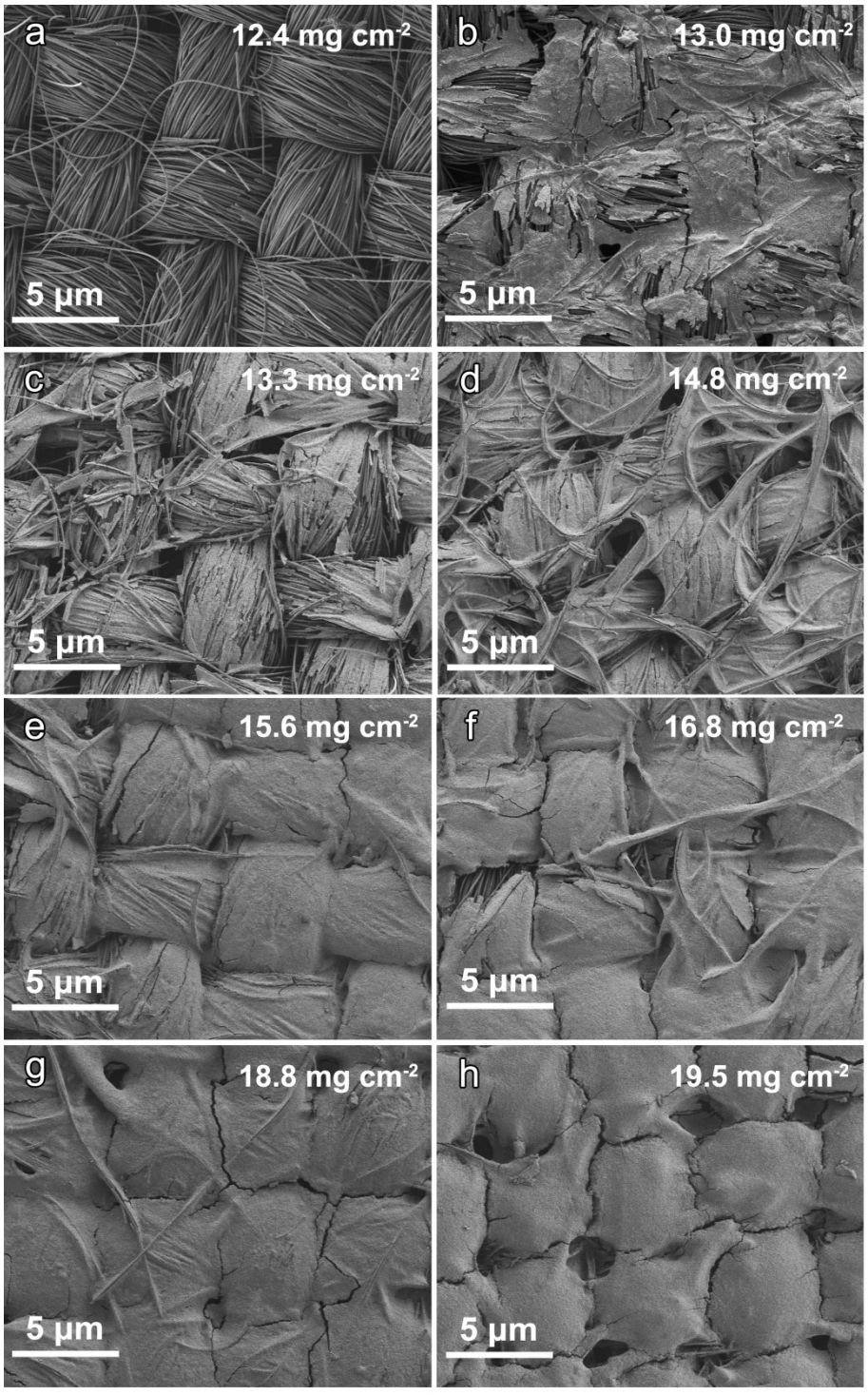

Figure S2. Top-view SEM images of (a) pure W0CC and (b-h) SiO@W0CC electrodes with different mass loading densities.

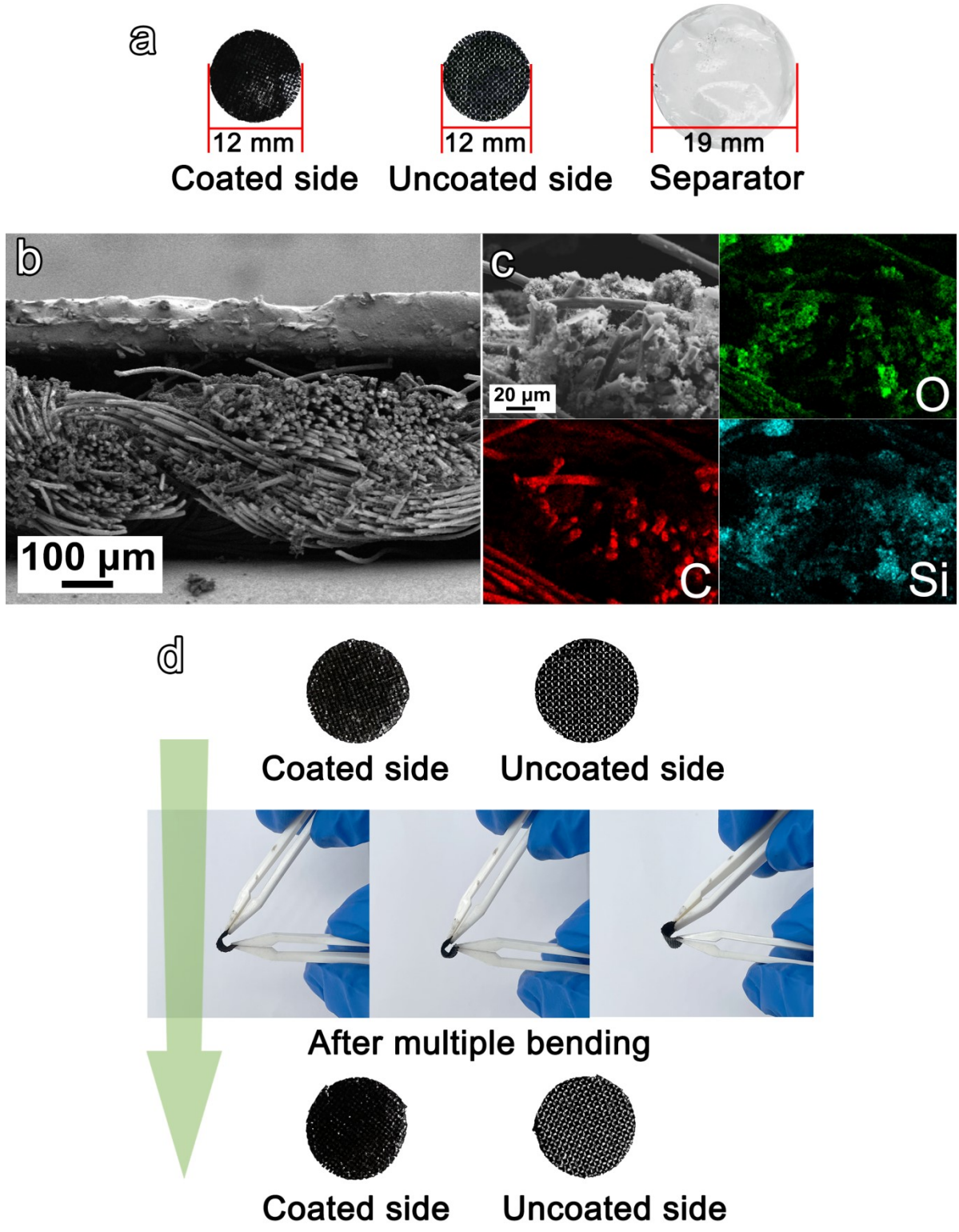

Figure S3. (a) Optical images of the SiO@W0CC electrode and separator obtained by dismantling a packaged coin cell after the rate performance test. (b) SEM image and (c) SEM

elemental mapping images of SiO@W0CC electrode obtained by dismantling a packaged coin cell after the cycling test. (d) Optical photographs of SiO@W0CC electrode with one side coated with active material and the other side without the active material before and after the bending test.

Note: It can be observed that the SiO@W0CC electrode of the coin cell, obtained by encapsulating, testing, and disassembling it, basically retains its original appearance, with only a small amount of material peeling off on the surface and just a trace amount of powder on the separator (Figure S3a). Additionally, the morphology and elemental distribution mapping of the SiO@W0CC electrode after the cycling test (Figure S3b-c) indicate that the structure of the electrode remains intact, and the SiO is still tightly bound to the W0CC. After that, we performed multiple bending tests on the SiO@W0CC electrode and took optical photographs for comparison. We discovered that after repeated bending, the electrode maintained its initial appearance and the SiO coating on the surface did not peel off (Figure S3d).

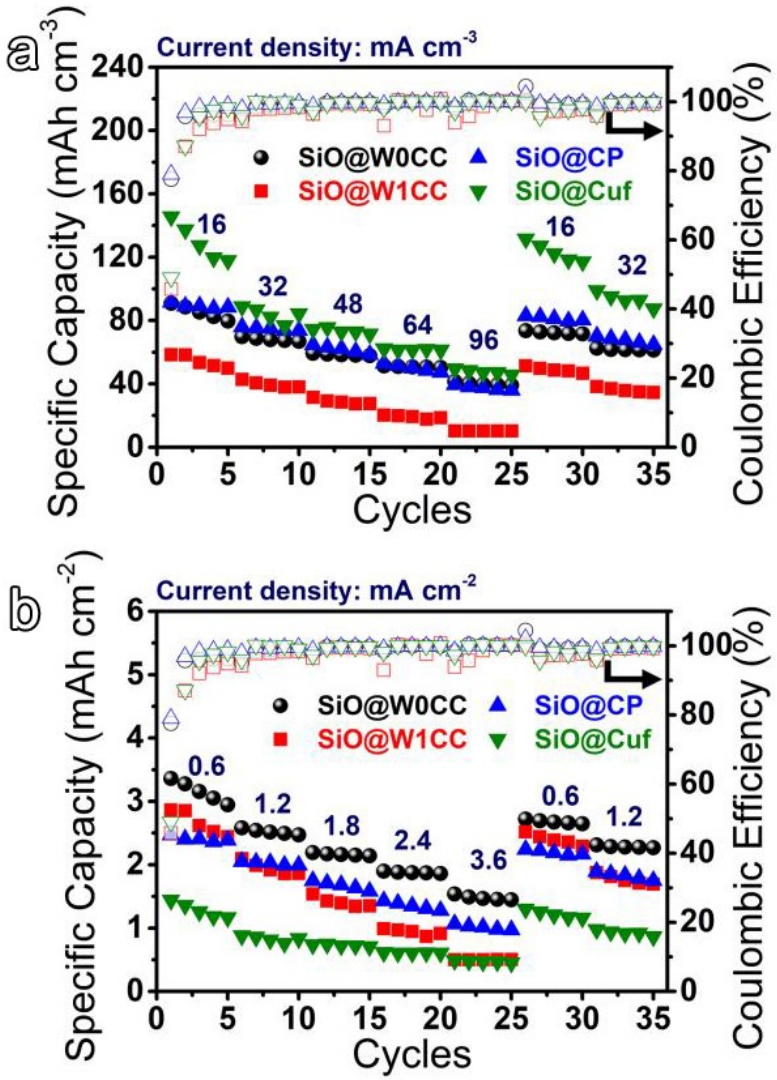

Figure S4. (a) Volumetric and (b) areal rate performance of SiO@W0CC, SiO@W1CC, SiO@CP, and SiO@Cuf electrodes with the same SiO loading density of 0.9 mg cm^{-2}.

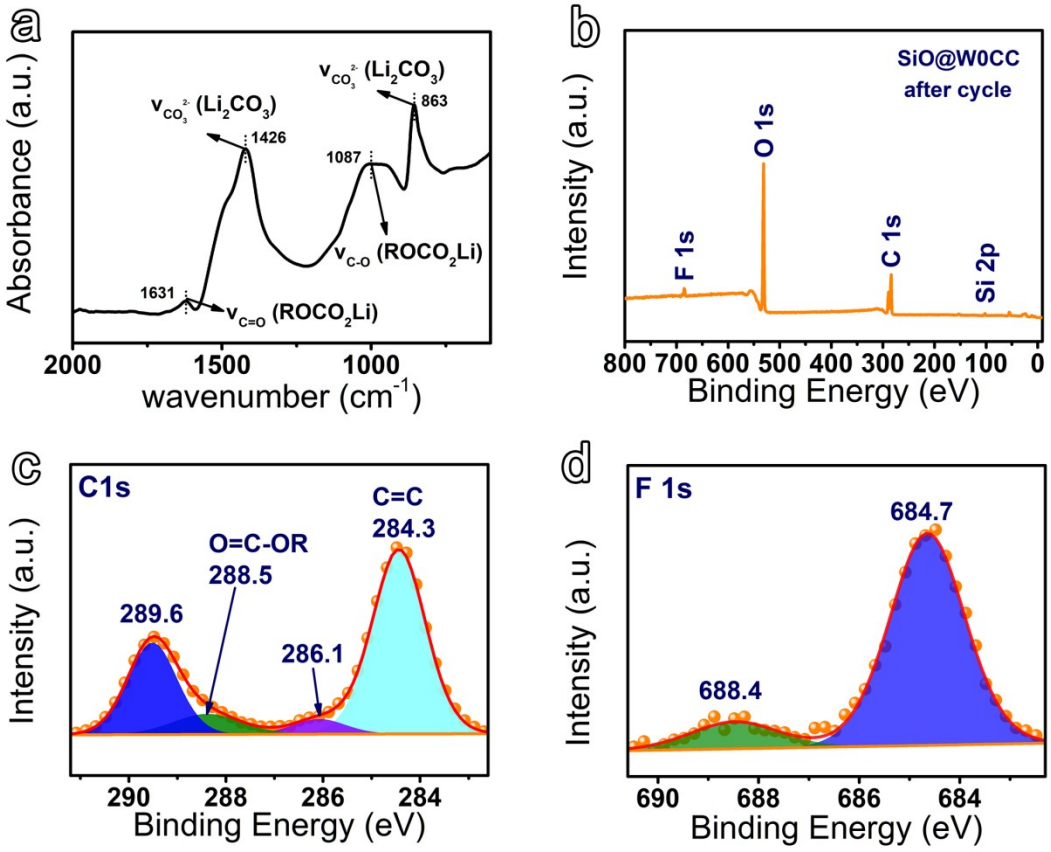

Figure S5. (a) FTIR spectra, (b) XPS full scan, (c) C 1s, and (d) F 1s XPS scans of SiO@W0CC electrode with the SiO loading density of 0.9 mg cm^{-2} after the cycling test.

Note: As shown in Figure S5a, the FTIR spectrum of the SiO@W0CC electrode after long cycling shows characteristic peaks attributed to $ROCO_2Li$ and Li_2CO_3, suggesting the presence of an SEI layer on the surface of the SiO@W0CC electrode after cycling. By comparing Figure S5b with Figure 2c, it can be observed that the Si signal on the outermost layer of the SiO@W0CC electrode after cycling becomes very weak, indicating that the retained SEI layer has covered most of the SiO active material. From the C 1s spectrum in Figure S5c, in addition to the inherent C=C (284.3 eV) and O=C-OR (288.5 eV) bonds of W0CC, characteristic peaks related to $ROCO_2Li$ (286.1 eV) and Li_2CO_3 (289.6 eV) are also observed. In the F 1s fine spectrum (Figure S5d), two peaks can be observed, with the peak at 684.7 eV originating from

LiF and the peak at 688.4 eV originating from $Li_xPF_y/LiPF_6$. These results fully support the existence of the SEI layer on the surface of the SiO@W0CC electrode after the cycling test, which is composed of $ROCO_2Li$, Li_2CO_3, and LiF.[4]

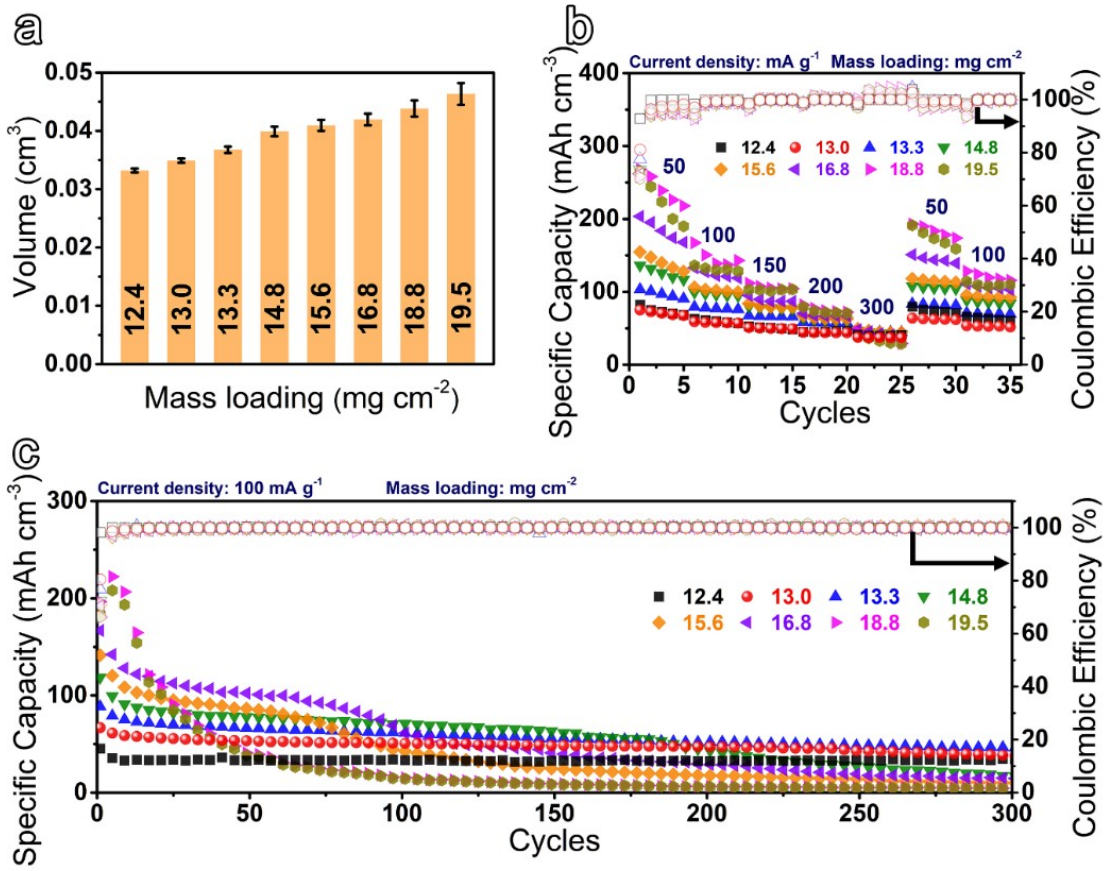

Figure S6. (a) Volume of SiO@W0CC electrodes under different loading densities. Comparisons of (b) volumetric-specific capacities and (c) cycle performance of SiO@W0CC electrodes with different mass loading densities.

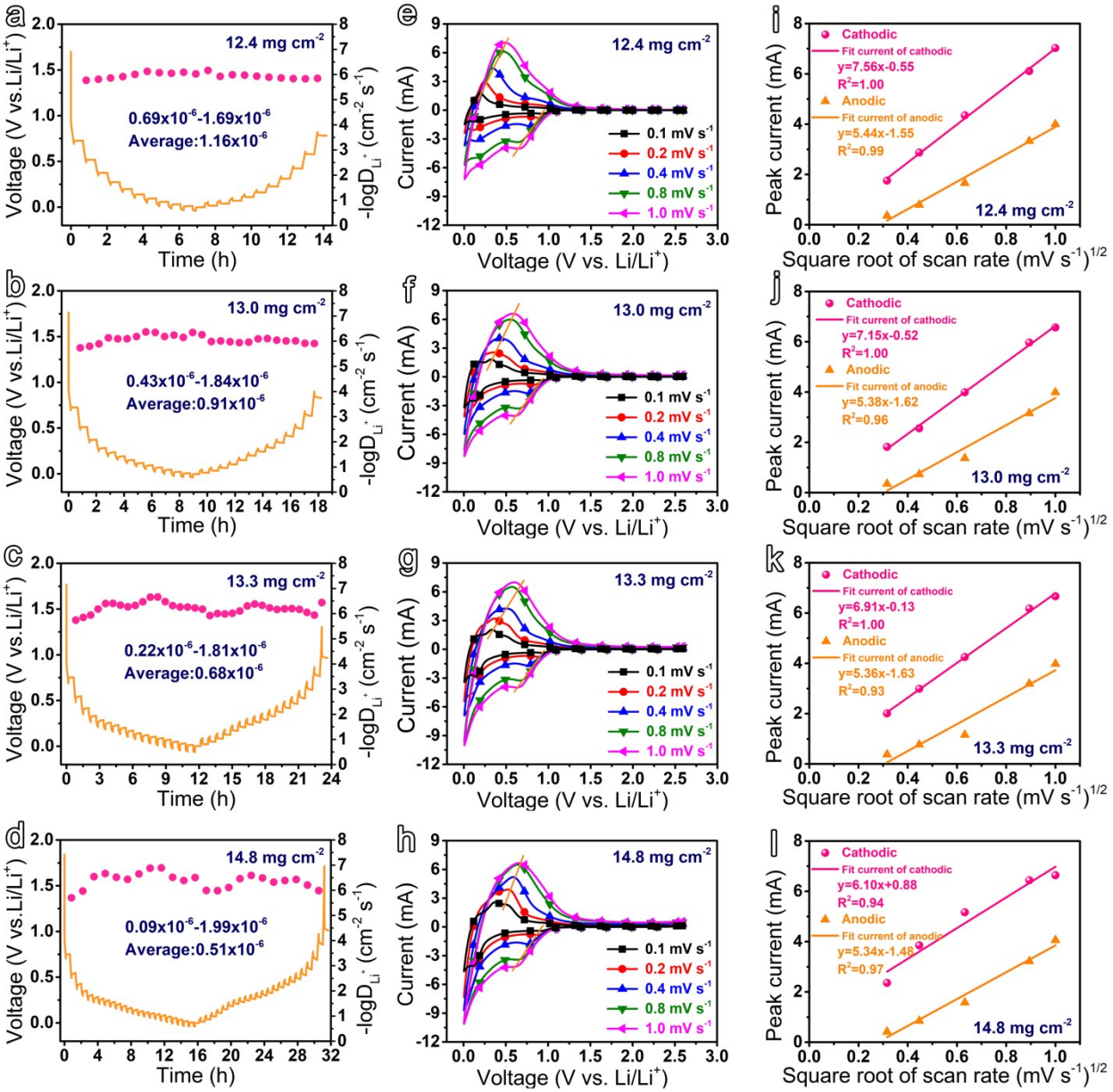

Figure S7. GITT curves of SiO@W0CC electrodes with mass loading densities of (a) 12.4, (b) 13.0, (c) 13.3, and (d) 14.8 mg cm^{-2}. CV curves at different scan rates of SiO@W0CC electrodes with mass loading densities of (e) 12.4, (f) 13.0, (g) 13.3, and (h) 14.8 mg cm^{-2}. The fitting curves between the peak current and the square root of the scan rate of CV curves at various scan rates for SiO@W0CC electrodes with mass loading densities of (i) 12.4, (j) 13.0, (k) 13.3, and (l) 14.8 mg cm^{-2}.

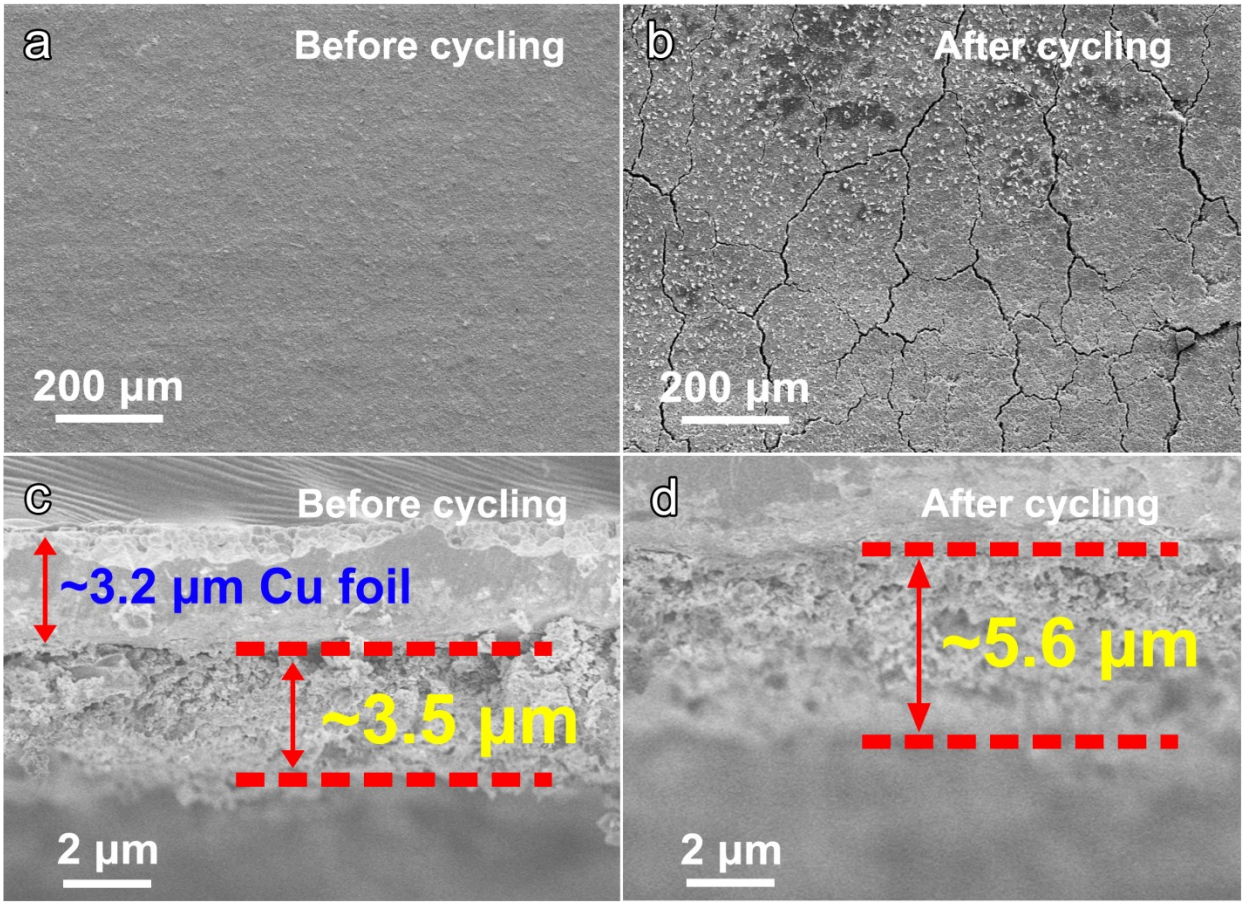

Figure S8. Top-view SEM images of SiO@Cuf electrode with the SiO loading density of 0.9 mg cm^{-2} (a) before and (b) after the cycling test. Cross-sectional SEM images of SiO@Cuf electrode with the SiO loading density of 0.9 mg cm^{-2} (c) before and (d) after the cycling test.

References for supporting information

1 Y. Fu, Y. Jin, J. Ma, J. Liu, Z. Wang, B. Wang and X. Gong, Lithium-ion transfer strengthened by graphite tailings and coking coal for high-rate performance anode, *Chem. Eng. J.*, 2022, **442**, 136184.

2 S. Guo, T. Koketsu, Z. Hu, J. Zhou, C.-Y. Kuo, H.-J. Lin, C.-T. Chen, P. Strasser, L. Sui, Y. Xie and J. Ma, Mo-Incorporated Magnetite Fe_3O_4 Featuring Cationic Vacancies Enabling Fast Lithium Intercalation for Batteries, *Small*, 2022, **18**, 2203835.

3 J. Pati, H. Raj, S. K. Sapra, A. Dhaka, A. K. Bera, S. M. Yusuf and R. S. Dhaka, Unraveling the diffusion kinetics of honeycomb structured $Na_2Ni_2TeO_6$ as a high-potential and stable electrode for sodium-ion batteries, *J. Mater. Chem. A*, 2022, **10**, 15460-15473.

4 W. Wang and S. Yang, Enhanced overall electrochemical performance of silicon/carbon anode for lithium-ion batteries using fluoroethylene carbonate as an electrolyte additive, *J. Alloy. Compd.*, 2017, **695**, 3249-3255.